Eur. Phys. J. B **36**, 619–626 (2003)
DOI: 10.1140/epjb/e2004-00016-2

THE EUROPEAN PHYSICAL JOURNAL B

KPZ equation with realistic short-range-correlated noise

M. Myllys[1], J. Maunuksela[1], J. Merikoski[1,a], J. Timonen[1], and M. Avikainen[2]

[1] Department of Physics, P.O. Box 35 (YFL), FIN-40014 University of Jyväskylä, Finland
[2] Metso Paper, P.O. Box 587, FIN–40100 Jyväskylä, Finland

Received 12 June 2003 / Received in final form 25 September 2003
Published online 30 January 2004 –

Abstract. We study a realistic simulation model for the propagation of slow-combustion fronts in paper. In the simulations the deterministic part of the dynamics is that of the KPZ equation. The stochastic part, including in particular the short-range noise correlations, is taken from images of the structure of real paper samples. The parameters of the simulations are determined by using an inverse method applied to the experimental front data and by comparing the simulated and the experimental effective-noise distributions. Our model predicts well the shape of the spatial and temporal correlation functions, including the location of the crossovers from short-range (SR) to long-range (LR) behavior. The values of the exponents $\chi_{\rm SR}$, $\beta_{\rm SR}$, $\chi_{\rm LR}$ and $\beta_{\rm LR}$ agree with the experimental ones. The apparent SR exponents are found to be the same for different types of quenched noise. The correlated noise is shown to have a major contribution to the effective, 'measured' nonlinearity. We discuss in detail how to implement the noise so as to obtain a realistic simulation model.

PACS. 05.40.-a Fluctuation phenomena, random processes, noise, and Brownian motion – 64.60.Ht Dynamic critical phenomena

1 Introduction

Kinetic roughening phenomena are usually classified into universality classes according to a few essential factors, i.e., the nature of the local front dynamics and symmetries or conservation laws [1,2]. Interfaces in each universality class display asymptotically unique scaling properties, which can be identified from the experimentally observed or simulated front data. Perhaps the most studied universality class of non-equilibrium phenomena is that of the nonlinear stochastic differential equation proposed by Kardar, Parisi and Zhang [3], or the KPZ equation. The KPZ equation can be argued to generically describe roughening processes that involve local propagation of an interface along its outward normal [2]. It has been applied to a wide variety of problems extending from propagating forest fires and magnetic flux fronts to growing bacterial colonies.

Previously, we have experimentally studied the kinetic roughening of one-dimensional smouldering fronts in paper samples. By measuring the scaling exponents of spatial and temporal correlation functions, universal amplitude relations, and persistence properties, we have unequivocally demonstrated [4–7] that this process asymptotically obeys KPZ dynamics. In what follows, we shall concentrate on the (1+1)-dimensional KPZ equation which, for the function $h(x,t)$ that gives the location or 'height' of the front, is given by [3]

$$\frac{\partial h(x,t)}{\partial t} = \nu \frac{\partial^2 h(x,t)}{\partial x^2} + \frac{\lambda}{2}\left[\frac{\partial h(x,t)}{\partial x}\right]^2 + F + \eta \ , \quad (1)$$

where ν is the surface tension coefficient, λ is the strength of the nonlinearity, F is a constant driving 'force', and the function η contains all the noise that affect the dynamics.

The form of the noise term η is known to have a big influence on the scaling properties of the KPZ equation [2]. If it is annealed, i.e., of the form $\eta = \eta(x,t)$, Gaussian, and both spatially and temporally uncorrelated such that $\langle \eta(x,t) \rangle = 0$ and $\langle \eta(x,t)\eta(x',t') \rangle = 2D\delta(x-x')\delta(t-t')$, then the scaling behaviour of stationary fronts is described by the values of the scaling exponents $\beta = 1/3$ and $\chi = 1/2$ (for the definitions of β and χ see Ref. [2] and Sect. 5 below). For λ=0, equation (1) reduces to the Edwards-Wilkinson equation (EW), which for this kind of noise can be solved exactly [1], with the result $\chi = 1/2$ and $\beta = 1/4$.

Uncorrelated noise may have a non-Gaussian amplitude distribution such as, *e.g.*, a power-law distribution $P(\eta) \sim \eta^{-(\mu+1)}$, where μ is a decay parameter [2]. In this case rare events with large amplitude can dominate the kinetics as the deterministic part of the dynamics is too 'slow' to suppress them. For μ below a critical value μ_c, the slower than Gaussian decay of noise amplitudes is asymptotically relevant, and the roughness exponent χ becomes proportional to μ. Usually power-law distributed

[a] e-mail: juha.merikoski@phys.jyu.fi

noise also breaks the simple self-affine interface morphology resulting in 'multi-affinity' characterized by an infinite series of exponents instead of just one [1].

Another possibility that may give rise to 'non-generic' scaling behavior is provided by annealed long-range-correlated noise [2]. If the noise is only spatially correlated, $\langle \eta(x,t)\eta(x',t')\rangle \sim |x-x'|^{2\rho-1}\delta(t-t')$, one finds $\chi = (1+2\rho)/3$ for $1/4 < \rho < 1$. For correlations decaying faster ($\rho < 1/4$), the usual KPZ values $\beta = 1/3$ and $\chi = 1/2$ are recovered. Situation is more complicated for temporally correlated noise, which breaks the Galilean invariance and also the scaling relation $\chi + \chi/\beta = 2$ [8].

In the case of quenched noise, which is of the form $\eta = \eta(x, h(x,t))$, the KPZ equation displays pinning for small values of the driving force F [9]. Depinning of the front is a critical phenomenon: at depinning the average front velocity begins to increase with a power law $v \sim (F - F_c)^\theta$ as F is increased above a critical value F_c. Below F_c, the front becomes pinned to one of the many locally stable configurations. At $F = F_c$, the scaling properties of the pinned front depend on the behavior of the nonlinear term resulting in two new universality classes. In the 'quenched KPZ' (QKPZ) universality class the effective nonlinearity diverges at the pinning transition, and the front can be mapped onto the directed percolation depinning (DPD) problem [10,11]. The scaling exponents for pinned fronts are then $\chi = \beta \approx 0.63$. On the other hand, if the nonlinearity vanishes at $F = F_c$, the asymptotic dynamics is described by the linear 'quenched' EW (QEW) equation with the exponents $\chi \approx 1$ and $\beta \approx 0.88$ for the pinned as well as for moving fronts just above F_c [9]. Quenched noise together with the nonlinearity naturally lead to a power-law distributed effective noise, and the fronts thus display 'multi-affine' scaling properties [1]. In the QKPZ case just above F_c, the second moments of the height-height correlation functions scale with exponents $\chi \approx 0.75$ and $\beta \approx 0.75$, but the fronts are not self-affine [12]. With a driving force strong enough, $F \gg F_c$, the front no longer can be pinned by the local disorder, and KPZ with uncorrelated noise is asymptotically recovered [12].

Attention of the theoretical and numerical work has so far been focussed on simple model systems with rather ideal types of correlated noise [1–3,8–14]. However, experimental systems are always restricted in size and often dominated by 'anomalous' noise. Therefore, the variation in the values measured for the scaling exponents in different experimental systems expected to be of KPZ type is large [2]. In the present work, we use direct numerical solution of the KPZ equation with noise determined from real paper samples to gain insight into the origin of the short-range dynamics observed in our slow-combustion experiments [4–7]. Other simulation parameters are determined by using an inverse method applied to the experimental front data. Like in the experiments, we find KPZ behavior in the long-range (LR) regime. The deviations from that in the short-range (SR) regime can originate from the noise as well as from other dynamical processes involved. This interplay of the 'stochastic' and 'deterministic' ingredients of the dynamics will be the focus of the present study.

First, in Section 2 we present a discretization of the KPZ equation and discuss its limitations. The input noises used in the simulations and their characteristics are discussed in Section 3. In Section 4 we describe the inverse method used to obtain input parameters for our simulations from the experimentally observed kinetics. The simulation results and their scaling behaviors are discussed in Section 5.

2 Discretization of the KPZ equation

In this work numerical solution of equation (1) was achieved by using the Euler's method solution of the finite difference equation

$$\begin{aligned} h_i^{n+1} = h_i^n &+ \nu_0 \frac{\Delta t}{\Delta x^2}(h_{i+1}^n + h_{i-1}^n - 2h_i^n) \\ &+ \lambda_0 \frac{\Delta t}{6\Delta x^2}\Big[(h_{i+1}^n - h_i^n)^2 + (h_i^n - h_{i-1}^n)^2 \\ &+ (h_{i+1}^n - h_i^n)(h_i^n - h_{i-1}^n)\Big] \\ &+ c_0 \Delta t + \sqrt{2D_0 \Delta t/\Delta x}\ \xi(i, h_i^n), \quad (2) \end{aligned}$$

where h_i^n is the front position at the ith lattice point at the n'th time step, ν_0, λ_0 and D_0 are the nominal values of the KPZ parameters used in the numerical integration, c_0 is the constant driving velocity (becomes the F of Eq. (1) in the continuum limit), and $\xi(i, h_i^n)$ is a two-dimensional noise matrix. In the simulations the value of the noise for a given (not discrete) value of h_i^n, was obtained from the noise matrix $\xi(i, h_i^n)$ as a linear interpolation. For the nonlinear term we use in equation (2) the 'improved discretization' introduced by Lam and Shin [15] to produce the correct renormalization of the KPZ parameters under coarse-graining. The spatial resolution Δx of the simulations was set to be the same as the resolution in our experiments (see below). The temporal resolution Δt was set small enough to ensure the numerical accuracy of the integration.

One should note that in the presence of quenched noise, for small values of Δt the simulated fronts can reach a pinned, non-propagating configuration of $h(x,t)$, in which the noise contribution and the other terms in equation (2) locally have exactly opposite values. This happens as for increasing temporal resolution Δt in the discretized equation, the noise term proportional to $\sqrt{\Delta t}$ vanishes more slowly than the other terms, which are proportional to Δt. To create a realistic simulation model with this type of noise, the input parameters ν_0, λ_0, D_0 and c_0 thus have to be determined (see Sect. 4 below) separately for each Δt.

We also tried other possible discretizations of the nonlinear term, the most simple version of which is the standard discretization $\frac{1}{2}\lambda_0 \Delta t (h_{i+1}^n + h_{i-1}^n)^2/4\Delta x^2$ [16]. The small-slope assumption behind the KPZ equation was studied by replacing in equation (2) the nonlinear term

with the expression $\lambda_0 \Delta t \sqrt{1 + (h^n_{i+1} + h^n_{i-1})^2/4\Delta x^2} - \lambda_0 \Delta t$. Here $-\lambda_0 \Delta t$ is needed to compensate for the exclusion of the constant term in the Taylor expansion of $\sqrt{1 + (dh/dx)^2}$, which arises when the local propagation of the front is in the direction of the normal [2]. Note that this square-root form contains all even powers of dh/dx. Additional tests were performed to study the possible finite-size effects in the LR scaling, and in the results of the inverse method, by using free and periodic boundary conditions. In our simulations (with rather limited statistics because of the availability of input noise data, see below) we found no noticeable differences between the results produced by different versions of the nonlinearity and boundary conditions. We also considered the possible role of a term of the type d^4h/dx^4, but no better 'fit' with the experimentally observed [6] SR dynamics could be obtained in this way.

3 Input noise in the simulations

The noise matrices used in the simulations were obtained from paper samples of the same grades as used in the experiments of references [4–7]. Parts of noise matrices are shown in Figure 1. Noise (I) is an optically scanned image of thin lens paper with basis weight 9.1 g/m^2. Ten different samples of the lens paper with size 210×540 mm^2 were scanned using 8 bit pixel depth and 250 dpi (0.102 mm/pixel) resolution. Noise (II) and noise (III) are β -radiographs of copier papers with basis weights 70 g/m^2 and 80 g/m^2, respectively, of size 177×455 mm^2. Two of the (II) 70 g/m^2 and three of the (III) 80 g/m^2 β -radiographs were scanned using 16 bit pixel depths and with a spatial resolution of 300 dpi (0.085 mm/pixel). Production of β radiographs is much more laborous in practice than optical scanning and, therefore, our statistics (disorder averaging) is better for noise (I) than for (II) or (III). Noise (IV) was generated by disordering or randomly scrambling the pixels of the noise matrix (I). The spatial resolution of the scanned images was chosen to be same as in the experiments [6]. We also tested simulations with higher spatial resolution, with no considerable changes in the results.

In the case of lens paper, the grey scale values of the scanned images were multiplied by -1 to make the local propagation velocity in the simulations a decreasing function of the mass density, as observed in real burning experiments. Naturally, the dependence of the front velocity on the local mass is somewhat more complicated in reality, but out main interest here is the effect of correlations in the noise. The variance of each matrix was set to unity and the systematic error caused by the scanner was corrected by setting to zero the mean of every column in the noise matrices.

Scanned noises (I), (II) and (III) were used in the simulations with the ordinary discretization of the KPZ equation equation (2). Noise (I) was also used in tests with the square-root form of the nonlinear term. Scrambled noise (IV) was used in simulations as both quenched [denoted by Q(IV) below] and annealed [denoted by A(IV)] noise. We used noise (I) also to study the effect of a rough initial condition and in a set of simulations, in which the value of velocity c_0 was varied.

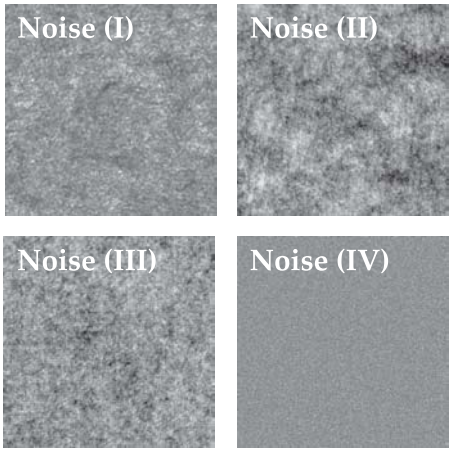

Fig. 1. 30×30 mm^2 samples of the noise used in the simulations. Noise (I) is an optically scanned image of lens paper, and noise (II) and noise (III) are β-radiographs of copier papers. Noise (IV) is generated by disordering noise (I).

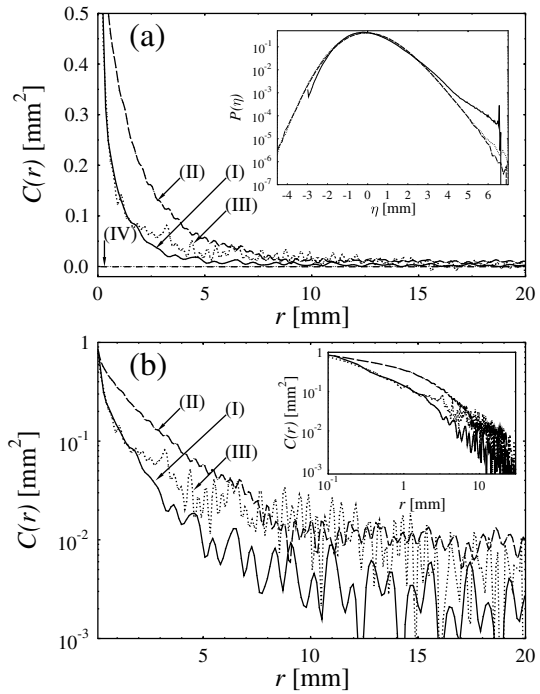

Fig. 2. The noise fluctuation correlation functions $C(r)$ for noises (II), (III), (I) and (IV) from top to bottom in linear (a) and in semi-logarithmic (b) scale. The inset of (a) shows the noise amplitude distributions and the inset of (b) a double-logarithmic plot of the correlation function.

In Figure 2a we show the two-point fluctuation correlation functions of the four input noises and the amplitude distributions of the noises in the inset. In the correlation functions averaging was only taken in the x direction. Correlations vanish in the scale of a few millimeters for all

noises except, of course, for the uncorrelated randomized noise (IV), for which the correlation length is of the order of one pixel size or Δx. Thereafter, for noises I-III the correlation functions appear to have power-law tails as is evident from the inset of Figure 2b. The regular density oscillations seen in Figure 2b in the scale of a few millimeters are a real feature resulting from the manufacturing process of paper (so-called 'wire marking').

4 Inverse method and input parameters

The nominal values for the simulation parameters ν_0 and λ_0 were obtained by using the inverse method of Lam and Sander [17] applied to our experimental front data [18]. Also, the simulated fronts were analysed in the same way to obtain the effective values of the parameters. Both results are presented in Figure 3. In this method [17] the coefficients of the KPZ equation are calculated as functions of coarse graining. First, equation (1) is discretized as

$$\frac{\Delta h_i(t)}{\tau} \simeq \mathbf{a} \cdot \mathbf{H}_i(t) + \eta_i(t), \qquad (3)$$

where τ is the discretization time step (a multiple of the recording time step), $\mathbf{a}$ is a vector of the coefficients of the KPZ equation, $\mathbf{a} = [c, \nu, \lambda/2]$, the vector $\mathbf{H}_i(t) = [1, \nabla^2 h, (\nabla h)^2]$ contains the coarse-grained derivatives of the front height, and $\eta_i(t)$ is here assumed to be Gaussian white noise. Spatial coarse graining is done by truncating the Fourier components with wavelengths smaller than ℓ from the recorded front heights $h(x,t)$. The vector $H_i(t)$ is calculated from the coarse-grained front heights for different time steps τ, and the vector of the coefficients $\mathbf{a}$ is determined by minimizing the function $\mathcal{J}(a) = \langle[\Delta h_i(t)/\tau - \mathbf{a} \cdot \mathbf{H}_i(t)]^2\rangle_{i,t}$. The noise correlator D is determined from the relation $D = (\ell\tau/2)\mathcal{J}(a_{\min})$ with $a_{\min}$ the solution of the minimizing problem [18].

For c_0 and D_0 the nominal values were fixed by comparing the velocity distributions of simulated and observed fronts. The values for c_0 are close to the average velocities in the experiments except for the 'unphysical' scrambled noise (IV), for which we for convenience chose $c_0 = 5.5$ mm/s for the quenched, and $c_0 = 24$ mm/s for the annealed noise.

The role of noise correlations in the effective (observed) λ was studied by performing simulations for $\lambda_0 = 0$, 2, 4, 8, and 12 mm/s, and then using the inverse method on the simulation data, see Figure 4. Clearly, there is a contribution to the effective nonlinearity from the correlated noise as well. For our most physical or the 'best simulation model', we in this case finally chose $\lambda_0 = 2$ mm/s to produce an effective λ close to the experimental value $\lambda_{\rm exp} = 4$ mm/s. It is easy to understand that in the case of a correlated noise matrix, the effective D and the nominal value D_0 can be very different, i.e. approximately $D_0 \simeq \Delta x/\Delta t I_{xy}$, where I_{xy} is the integral of the noise correlation function $C(r)$ from zero up to the apparent correlation length of the noise.

The nominal values for the coefficients used in the main part of this study are shown in Table 1 for one of the copier papers (80 g/m^2) and for the lens paper. The quoted values are averages over coarse-graining lengths $\ell \in$ [15,20] mm, and determined for the shortest coarse-graining times τ used. For the determination of c and λ, smaller values of τ can and have been used, see reference [18] for a detailed discussion.

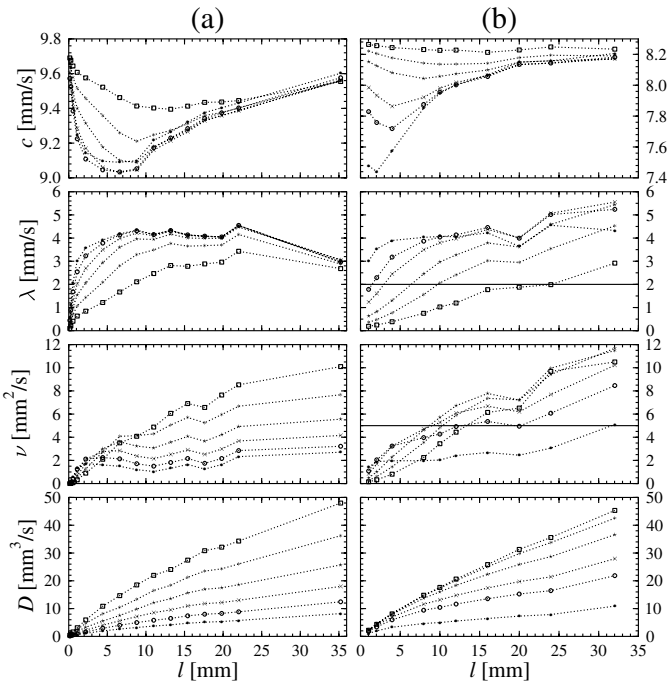

Fig. 3. The effective values of the KPZ parameters as determined by the inverse method. (a) On the left we show the experimental values and (b) on the right the values determined from the simulated fronts produced by our 'best simulation model' (noise II). The nominal values λ_0 and ν_0 are indicated by the horizontal lines in (b). The values of the time steps are τ= 0.2(.), 0.4(∘), 0.8(×), 1.6(⋆),3.2(*) and 6.4(□) s.

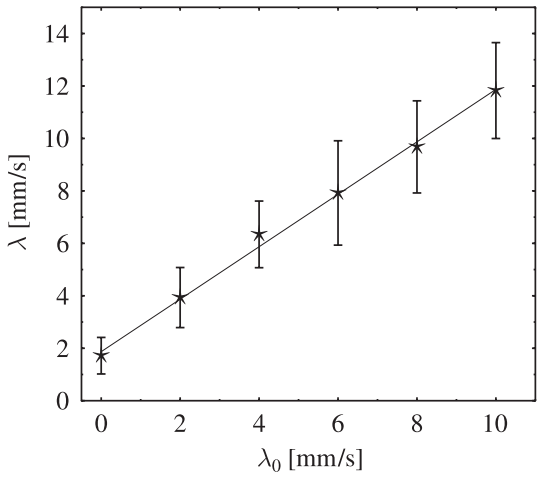

Fig. 4. The strength of the nonlinearity λ calculated from the simulation data as a function of the nominal value of λ_0. The slope of the fitted line is one.

Table 1. Nominal values of the KPZ coefficients in the simulations of copier paper [noise (II)] and lens paper [noise (I)].

Noise	c_0 $[\frac{\mathrm{mm}}{\mathrm{s}}]$	λ_0 $[\frac{\mathrm{mm}}{\mathrm{s}}]$	ν_0 $[\frac{\mathrm{mm}^2}{\mathrm{s}}]$	D_0 $[\frac{\mathrm{mm}^3}{\mathrm{s}}]$
(I)	11.4	2.0	5.0	0.005
(II)	0.45	0.3	0.1	0.0000045

5 Scaling properties of simulated fronts

For the simulation data we performed data analysis similar to the one done earlier in our experimental work described in detail in reference [6], except that the removal of the global tilt from simulated fronts was not necessary as we normalized the average of each column of the noise matrix to get rid of the systematic error produced by the optical scanner.

According to the Family-Vicsek [19] scaling relation the (squared) front width $w^2(L,t) \equiv \langle\overline{(h-\bar{h})^2}\rangle$, where the overbar denotes spatial and brackets noise averaging, should scale as a function of time t and system size L as

$$w^2(t) \sim t^{2\beta} f(t/L^z) \sim \begin{cases} t^{2\beta} & \text{, for } \xi \ll L; \\ L^{2\chi} & \text{, for } \xi \gg L. \end{cases} \quad (4)$$

Here $\xi \sim t^{1/z}$ denotes the correlation length, which increases with time until it saturates due to finite system size. The evolution of the front width in our simulations is shown in Figure 5. The solid line denotes the front width $w^2(t)$ averaged over ten simulations starting from flat initial conditions. The dashed line is the evolution of ten simulations with the same noise but with different rough initial conditions. The guideline in Figure 5 corresponds to the theoretical value for the growth exponent in the asymptotic regime, $\beta = 1/3$. The inset shows the magnitude of the fluctuations for ten independent simulations with noise (I). The saturation values of w_{sat} were almost equal to the experimental ones [6]: $w^2_{\mathrm{sat}} \simeq 10$ mm^2 for noise (I) corresponding to the lens paper and $w^2_{\mathrm{sat}} \simeq 4$ mm^2 for noises (II) and (III) determined from the copier papers.

Another way to determine the scaling exponents is to study the stationary two-point correlation function [2] of front height fluctuations $\delta h(x,t)$ around the mean $\bar{h}(t)$,

$$C_2(r,t) = \langle\overline{[\delta h(x',t') - \delta h(x'+r,t'+t)]^2}\rangle_{x',t'}, \quad (5)$$

where $\delta h(x,t) = h(x,t) - \overline{h(t)}$. We consider the spatial and temporal correlations separately via

$$G(r) \equiv C_2(r,0) \sim r^{2\chi} \quad \text{and} \quad C(t) \equiv C_2(0,t) \sim t^{2\beta}. \quad (6)$$

In Figure 6a we show the spatial correlation function $G(r)$ for noises (I), (II), (III), A(IV), and Q(IV). Like in our experiments [6], distinct crossovers to asymptotic scaling are evident, except in the result for noise A(IV). The slopes of the guidelines in the figure are taken from the experimental results and match well the simulated results. For the short-range regime we find $\chi_{\mathrm{SR}} \sim 0.9$ and for the long-range (asymptotic) regime $\chi_{\mathrm{LR}} \sim 0.5$. We note that $G(r)$ displays quite a short asymptotic scaling regime if the simulations are started from flat initial conditions. This is because of the limited size of the 'paper' (scanned noise matrix) in the simulations. Increasing the nonlinearity and starting from a rough initial configuration speeds up roughening, and facilitates a more accurate determination for χ_{LR}. The temporal correlation functions $C(t)$ for the same simulations are shown in Figure 6b. Again, the slopes of the guidelines are taken from experiments [6], and correspond to $\beta_{\mathrm{SR}} = 0.7$ and $\beta_{\mathrm{LR}} = 0.33$.

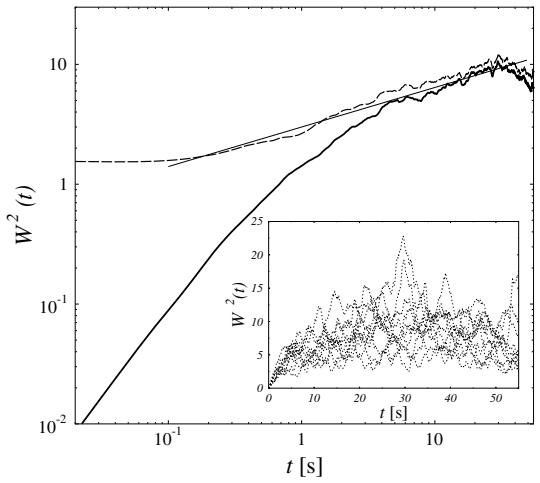

Fig. 5. The average front widths w^2 as functions of time for ten simulations with noise (I). The result for a flat initial condition is plotted with a thick solid line, and with a dashed line for rough initial conditions. The inset displays the magnitude of fluctuations, showing the individual results for ten realizations of noise (I).

In Table 2 we show the crossover points r_c and t_c for spatial and temporal correlation functions, respectively. There is a considerable uncertainty in r_c and t_c because of the rather limited noise averaging, so our conclusions on them will be rather qualitative. First, the values r_c and t_c produced by the simulation models are reasonably close to those measured in the experiments [6]. However, in contrast with the experiments, in simulations we observe no multiscaling in the correlation functions, i.e. strong dependence on the moment (for details see Refs. [5,6], in particular Fig. 1 in [5] and Fig. 8 in [6]). As expected, simulations with randomized annealed noise A(IV), display no crossover. The second question concerns the origin of the crossovers. By comparing simulations (I) (and also (I') and (I")) we observe that, for the given noise correlations, the spatial crossover scale r_c is not very strongly dependent on the simulation parameters or on $\langle v\rangle$. We conclude that r_c is mainly determined by the correlations in the input noise. In the rightmost column of Table 2 we show the dimensionless ratio $\langle v\rangle t_c/r_c$. Within the accuracy of the crossover values, we find that $r_c \sim t_c\langle v\rangle$, where the constant of proportionality is close to unity [20]. This result is in agreement with r_c being mainly determined by the input-noise correlations, as asymptotic scaling would in this case be expected for times $t > r_c/\langle v\rangle$.

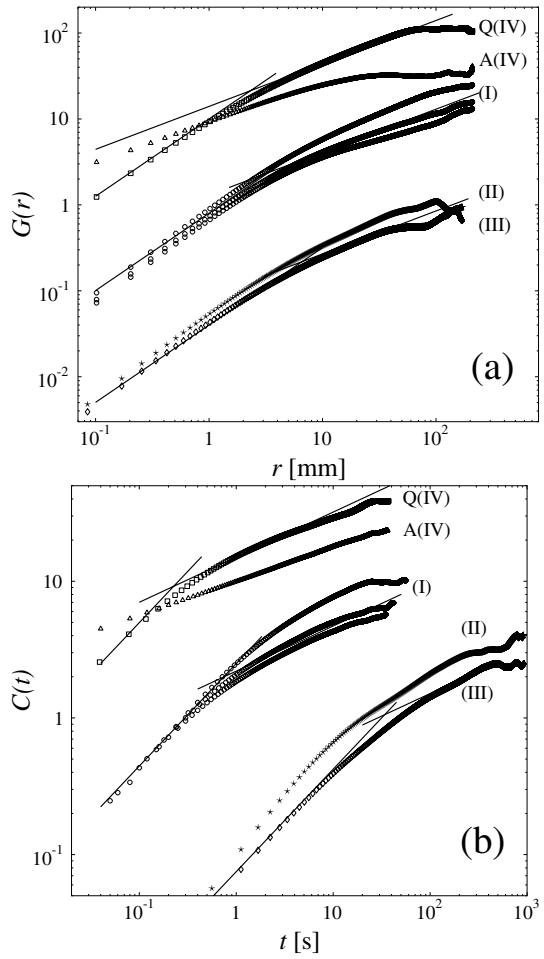

Fig. 6. (a) Correlation functions $G(r)$ for five different noises. The solid lines correspond to the experimentally observed scaling exponents ($\chi_{\rm SR} = 0.9$ and $\chi_{\rm LR} = 0.5$). (b) Correlation functions $C(t)$ for the same noises. The solid lines correspond to the experimentally observed scaling exponents ($\beta_{\rm SR} = 0.7$ and $\beta_{\rm LR} = 0.33$). For comparison, we whow for noise (I) the correlation functions for three different values of the driving velocity, curves from top to bottom have $c_0 = 8.4$, 11.4, and 13.4 mm/s, respectively. Of these $c_0 = 11.4$ mm/s is our 'best simulation model' for the lens paper. For clarity, the data sets (II), (III), and (IV) have been shifted in (a) by factors 0.1, 0.1 and 15, and in (b) by factors 0.7, 0.7 and 10, respectively.

Table 2. Average velocity $\langle v \rangle$ of the front in the stationary state and the locations of the crossovers from SR to LR behavior for the correlation functions shown in Figure 6. We also show data for additional simulations (I') and (I"), where the simulation parameters are the same as for noise (I) in Table 1 except that in (I') $c_0 = 13$ mm/s and $D_0 = 0.001$ mm^3/s, and in (I") $c_0 = 8$ mm/s and $D_0 = 0.01$ mm^3/s. The parameters in (I') and (I") were chosen so as to produce the same value of $\langle v \rangle$ and the same width of the input noise amplitude distribution as in our 'best simulation model' for the lens paper. For the simulation set Q(IV') the parameters were the same as for Q(IV) except that $c_0 = 12.3$ mm/s and $D_0 = 0.01$ mm^3/s,

Noise	c_0 [$\frac{\rm mm}{\rm s}$]	$\langle v \rangle$ [$\frac{\rm mm}{\rm s}$]	r_c [mm]	t_c [s]	$\langle v \rangle t_c / r_c$
(I)	8.0	4.5	5.8	2.3	1.8
(I)	11.4	8.0	5.2	0.75	1.2
(I)	18.0	15.6	3.2	0.40	2.0
(I')	13.0	8.0	4.0	0.78	1.6
(I")	8.0	8.0	4.2	0.51	0.98
(II)	0.45	0.45	2.9	11	1.7
(III)	0.45	0.45	2.8	14	2.3
Q(IV)	24.0	9.1	2.5	0.50	1.8
Q(IV')	12.3	9.1	1.0	0.23	2.1

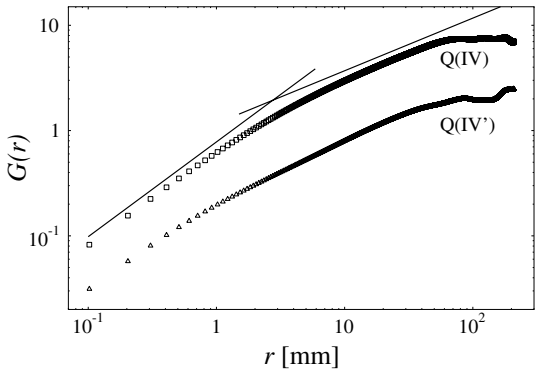

Fig. 7. Correlation functions $G(r)$ for noise IV with two sets of parameters, cases Q(IV) and Q(IV') in Table 2.

For randomized but quenched noise Q(IV), crossover-like behavior is observed at $r_c \approx 2.5$ mm. This length scale cannot be related to any length scale in the input noise, for which the correlation length in this case is of the order of one pixel (roughly 1 mm). The simulation parameters were chosen for this case so as to produce the same roughness of the stationary fronts as in the other cases, which meant the noise amplitude was now clearly higher. Therefore the fronts were much closer to the pinning limit than in the other cases, and an additional length scale related to 'distance' from pinning became visible. The crossover found for the Q(IV) case is related to this additional length scale. We tested the behaviour of the additional length scale by changing the simulation parameters for noise (IV) such that distance from pinning was increased. The resulting spatial correlation function is shown in Figure 7, and the spatial and temporal crossover parameters are shown in Table 2 as case Q(IV'). As expected, the apparent crossover scale was now reduced to $r_c \approx 1.0$ mm. We also noticed that this additional length scale, which is regulated by the distance from pinning, is related to the effective ratio D/ν (whose dimension is length), where D and ν are obtained from the simulated fronts by the inverse method which assumes annealed noise. For the simulation sets (I-III), the correlation length of the input noise was well *above* the effective ratio D/ν, and determined r_c as discussed above. We also note that, for the KPZ equation with annealed noise, the ratio D/ν only sets the amplitude (the transverse scale) of the asymptotic part of the spatial correlation function [2]. As only propagating fronts well above pinning were considered in the experiments [4–7],

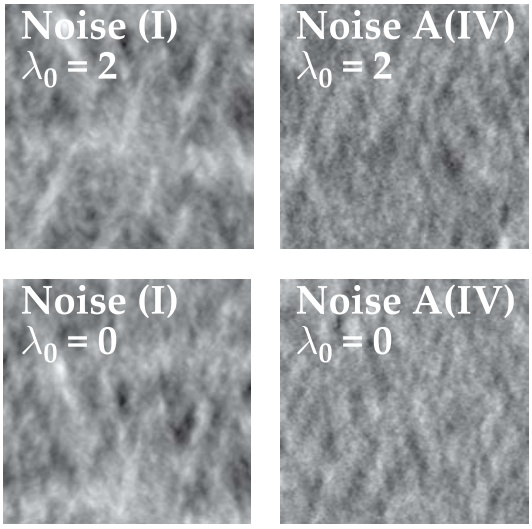

Fig. 8. Grey scale maps of $\eta_{\rm eff}(x,t)$ for $\tau = 4$ s. Lighter areas correspond to higher front velocities.

we do not analyze here the effects of pinning limit any further.

The effective noise $\eta_{\rm eff}$ can be determined from the fluctuations of the local front velocities as [21]

$$\eta_{\rm eff}(x,t) \equiv [\delta h(x,t+\tau) - \delta h(x,t)]/\tau, \qquad (7)$$

where $\delta h(x,t) = h(x,t) - \overline{h(t)}$ and τ is the time step. Grey scale images of $\eta_{\rm eff}(x,t)$ as produced by simulations for $\lambda_0 = 2$ and 0 mm/s are shown in Figure 8. The images on the left are for noise (I), and on the right for noise A(IV). There is no major qualitative difference between the noise maps for zero and finite λ_0, which is in agreement with the observation that quenched noise alone can produce an effective nonlinearity (see discussion of Fig. 4 above). From the noise maps we determined amplitude distributions $P(\eta_{\rm eff})$ for time steps $\tau = 1/2$, 1, 2, 4, and 8 s. In the experiments the noise-amplitude distributions had power-law tails for short time steps, but the simulations do not reproduce this feature. Again, this indicates that KPZ simulations of this kind cannot include all dynamical features of the real burning process. From the noise map, the two-point correlation function of the *effective* noise can be obtained via

$$C_\eta(x) = \langle \delta\eta_{\rm eff}(x_0+x,t_0)\delta\eta_{\rm eff}(x_0,t_0)\rangle, \qquad (8)$$

where $\delta\eta_{\rm eff}(x,t) = \eta_{\rm eff}(x,t) - \overline{\eta_{\rm eff}(t)}$, the overbar denoting spatial averaging at the given t. This function is shown in Figure 9 for the input noises (I) and A(IV) (the correlations in the input noises themselves were already shown in Fig. 2). The effective noise correlations for these two simulations are qualitatively (apart from the amplitudes) quite similar, despite the very different nature of the input noises. This indicates that, already in these time scales, the deterministic part of the equation of motion has a big effect on the dynamics, and front fluctuations largely appear the same way as those produced by annealed noise.

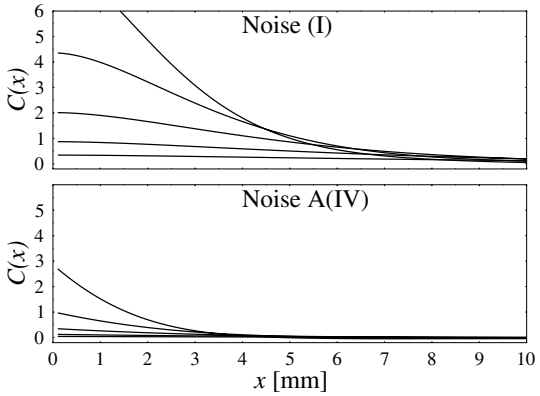

Fig. 9. Spatial effective noise correlations observed in simulations for input noises (I) and (IV). The time step used to determine the effective noise via equation (7) was $\tau = 1/2$, 1, 2, 4 and 8 s, from top to bottom.

6 Conclusion

We have studied a simulation model combining KPZ dynamics with realistic noise for the propagation of slow-combustion fronts in paper. In the simulations the deterministic part of the dynamics was taken to be that of the KPZ equation, with parameters determined by applying an inverse method to the experimental front data. The noise correlations were taken from images of the structure of real paper samples. For given values of the other simulation parameters (including the discretization), the noise amplitude was set by comparing the effective noise in the simulations with that in the experiments.

Our 'best simulation model' reproduces well the shapes of the spatial and temporal correlation functions and the location of the crossovers. The actual values of the exponents $\chi_{\rm SR}$, $\beta_{\rm SR}$, $\chi_{\rm LR}$ and $\beta_{\rm LR}$ agree with the experimental ones. For copier paper the agreement is perhaps less convincing than for the lens paper, possibly because of the rather limited noise averaging in the simulations. For propagating fronts well above pinning, the apparent SR exponents are roughly the same for all types of quenched noise. Notice that for noise IV the length scale related to structural noise is reduced to one pixel. Therefore an additional length scale regulated by closeness to pinning becomes visible, and the crossover in the spatial correlation function is now related to this scale. This additional length scale appears to be related to the effective D/ν value as determined by the inverse method.

The coarse graining of the effective KPZ coefficients in the simulations is similar to that seen in the experiments. The quenched SR correlated noise present in our model was shown in part to contribute to the effective nonlinearity, and taking into account this contribution turned out to be essential for the construction of a realistic model for the asymptotic behavior of the fronts.

Evidently the structural noise correlations do not alone explain all features of the data obtained from real burning experiments, in particular the apparent multiscaling in the short-range data and the power-law tails of the effective noise distributions. In addition to various manipulations

of the input noise, we studied the possible role of deterministic terms of the type $(dh/dx)^{2m}$ for $m > 1$, and the term d^4h/dx^4, in the equation of motion, as well as the effect of different boundary conditions, but no explanation for the apparent multiscaling (in the SR regime) seen in the experiments could be found that way. The origin of these features is beyond the present KPZ description, which does not take into account possible dynamical features in the noise such as *e.g.* the dynamical coupling of effective noise in convection and heat conduction.

This work has been supported by the Academy of Finland under the Center of Excellence Program (Project 44875) and the MaDaMe Program (Project 772495).

References

1. A.-L. Barabási, H.E. Stanley, *Fractal Concepts in Surface Growth* (Cambridge University Press, Cambridge, 1995)
2. T. Halpin-Healy, Y.-C. Zhang, Phys. Rep. **254**, 215 (1995)
3. M. Kardar, G. Parisi, Y.-C. Zhang, Phys. Rev. Lett. **56**, 889 (1986)
4. J. Maunuksela, M. Myllys, O-P. Kähkönen, J. Timonen, N. Provatas, M.J. Alava, T. Ala-Nissila, Phys. Rev. Lett. **79**, 1515 (1997)
5. M. Myllys, J. Maunuksela, M. Alava, T. Ala-Nissila, J. Timonen, Phys. Rev. Lett. **84**, 1964 (2000)
6. M. Myllys, J. Maunuksela, M. Alava, T. Ala-Nissila, J. Merikoski, J. Timonen, Phys. Rev. E **64**, 036101 (2001)
7. J. Merikoski, J. Maunuksela, M. Myllys, J. Timonen, M. Alava, Phys. Rev. Lett. **90**, 024501 (2003)
8. E. Medina, T. Hwa, M. Kardar, Y.C. Zhang, Phys. Rev. A **39**, 3053 (1989)
9. L.A.N. Amaral, A.-L. Barabási, H. Makse, H.E. Stanley, Phys. Rev. E **52**, 4087 (1995)
10. H. Leschhorn, L.-H. Tang, Phys. Rev. E **49**, 1238 (1994)
11. Z. Olami, T. Procaccia, R. Zeitak, Phys. Rev. E **49**, 1232 (1994)
12. H. Leschhorn, Phys. Rev. E **54**, 1313 (1996); H. Leschhorn, T. Natterman, S. Stepanow, L.-H. Tang, Ann. Phys. **6**, 1 (1997)
13. M. Beccaria, G. Gurci, Phys. Rev. E **50**, 4560 (1994)
14. M. Wu, K.Y.R. Billah, M. Shinozuka, Phys. Rev. E **51**, 995 (1995)
15. Chi-Hang Lam, F.G. Shin, Phys. Rev. E **58**, 5592 (1998)
16. K. Moser, J. Kertesc, D.E. Wolf, Physica A **178**, 215 (1991)
17. C.-H. Lam, L.M. Sander, Phys. Rev. Lett. **71**, 561 (1993)
18. J. Maunuksela, M. Myllys, J. Merikoski, J. Timonen, T. Kärkkäinen, M.S. Welling, R.J. Wijngaarden, Eur. Phys. J. B **33**, 193 (2003)
19. F. Family, T. Vicsek, J. Phys. A **18**, L75 (1985)
20. The mean-field-type result $r_c \sim t_c\langle v\rangle$ is expected to break close to the pinning transition [2]. In our experiments [6] and in the simulations reported here, we are well above the transition, which for our simulation model (I) we estimate to occur for $c_0 \approx 4$ mm/s
21. V. Horváth, F. Family, T. Vicsek, Phys. Rev. Lett. **67**, 3207 (1991)